Separation Science and Technology
Publication details, including instructions for authors and subscription information:
http://www.informaworld.com/smpp/title~content=t713708471

Molecular Modeling of Thiophene in the Vapor-Liquid Equilibrium

Francisco M. Juárez-Guerra[a]; José Luis Rivera[a]; Abel Zúñiga-Moreno[b]; Luis A. Galicia-Luna[b]; José Luis Rico[a]; Javier Lara[a]
[a] Facultad de Ingeniería Química, Universidad Michoacana de San Nicolás de Hidalgo, Morelia, Michoacán, México [b] Instituto Politécnico Nacional, ESIQIE-Graduados, Lab. de Termodinámica, México

To cite this Article Juárez-Guerra, Francisco M. , Rivera, José Luis , Zúñiga-Moreno, Abel , Galicia-Luna, Luis A. , Rico, José Luis and Lara, Javier(2006) 'Molecular Modeling of Thiophene in the Vapor-Liquid Equilibrium', Separation Science and Technology, 41: 2, 261 — 281
To link to this Article: DOI: 10.1080/01496390500446129
URL: http://dx.doi.org/10.1080/01496390500446129

Separation Science and Technology, 41: 261–281, 2006

ISSN 0149-6395 print/1520-5754 online
DOI: 10.1080/01496390500446129

Molecular Modeling of Thiophene in the Vapor–Liquid Equilibrium

Francisco M. Juárez-Guerra and José Luis Rivera
Facultad de Ingeniería Química, Universidad Michoacana de San Nicolás de Hidalgo, Morelia, Michoacán, México

Abel Zúñiga-Moreno and Luis A. Galicia-Luna
Instituto Politécnico Nacional, ESIQIE-Graduados, Lab. de Termodinámica, México

José Luis Rico and Javier Lara
Facultad de Ingeniería Química, Universidad Michoacana de San Nicolás de Hidalgo, Morelia, Michoacán, México

Abstract: Direct molecular dynamics simulations of the vapor–liquid interface of pure thiophene systems have been performed in order to study the interfacial and bulk properties of this molecule. The simulations were carried out using a new force field developed in this work. Vapor–liquid interfaces were simulated at temperatures between 300 and 500 K, and interfacial properties such as the coexistence densities, vapor pressure, surface tension, and interfacial thickness were calculated. Experimental liquid densities were measured at temperatures in the range of 293.31 and 352.44 K, and agreed well with the calculated results.

Keywords: Molecular modeling, thiophene, vapor–liquid equilibrium

Received 17 August 2005, Accepted 19 October 2005

Address correspondence to José Luis Rivera, Facultad de Ingeniería Química, Universidad Michoacana de San Nicolás de Hidalgo, Santiago Tapia No. 403, Col. Centro, Morelia, Michoacán, 58000, México. Tel.: +52 443 3273584 (108); Fax: +52 443 3273584 (102); E-mail: jrivera@posgrado.fiq.umich.mx

INTRODUCTION

The petroleum oil produced in the southeast part of Mexico has a high level of organo-sulfur compounds (1). The oil produced in the northeast part of this region contains mainly alkylbenzothiophenes while in the southeast part alkyldibenzotiophenes. If these compounds are not extracted from the refined oil products like gasoline and diesel, they will damage animal health, crops, timber, and even buildings through acid rain (2). The organo-sulfur compounds start causing problems even during extraction in the oil wells, where these compounds along with hydrogen sulfide and water molecules adhere to the inner wall and eventually block the oil flow through the well (3). Hydrodesulfurization processes are commonly used in refineries to hydrogenate these organo-sulfur compounds and extract the sulfur in the form of hydrogen sulfide. Such processes use bi- and tri-metallic catalysts often made of Ni, Co and Mo (4, 5), and process conditions between 1.38–20.70 MPa and 560–700 K, depending on the fuel processed (6). The actual regulations in North America for sulfur content in fuels are 350 ppm in gasoline (7), and 500, 5000 and 3000 ppm by weight (upper limit) for highway diesel, non-road diesel and jet fuel respectively (8). By 2006 there will be reductions in these levels and the new limits will be 30 ppm in gasoline (7), 15 and 500 ppm by weight for highway and non-road diesels respectively, and there will be no change in the levels of jet fuel (8). These new regulations seem difficult to reach without new catalysts or processes (6). Alternative approaches to separate the sulfur compounds from the fuels are biodesulfurization (9, 10), catalytic oxidation combined with ultrasonication and solvent extraction (11), sonochemical decomposition (12), adsorption with activated carbon (13), with hydrogels (14) and some studies had shown that organo-sulfur compounds can be extracted selectively using supercritical extraction processes (15).

In the literature, there are several theoretical studies dealing with the structure and intermolecular interactions of thiophene and its derivates (16–20). Density functional theory (DFT) and Restricted Hartree-Fock (RHF) calculations have been employed by Kupka et al. (16, 17) and Kochikov et al. (18) to study the geometry and the spectra (IR and Raman) of 3-methylthiophene, thiophene and its mixture with acetonitrile; they reported a good agreement with the experimental data in gas and condensed phases. They also found that DFT calculations produced results closer to experiment than the corresponding RHF calculations for bond lengths, dipole moments, rotational constants and harmonic frequencies (16). Dibenzothiophene had also been studied with these methodologies to obtain the geometry, electronic structure, and polarizability of this molecule and the results were compared with measured values; the study found a difference of 3% with the experimental values (19). The intermolecular interactions of thiophene dimers have been evaluated with ab initio

molecular orbital calculations and that study concluded that the substantial attractive interaction between two molecules of thiophene is due to electrostatic and dispersion interactions and there are no charge transfer interactions (20).

To our knowledge, there are no reported studies of specific interaction potentials for thiophene or its derivates. In this initial study we developed a new interaction potential for thiophene, the smallest cyclic organo-sulfur compound found in oil. This potential was developed performing DFT calculations to find the parameters of a potential consisting of analytical functions representing the electrostatic and intramolecular interactions. This potential was used to simulate thiophene in the vapor–liquid equilibrium region using the molecular dynamics methodology (21). Liquid densities were also measured experimentally in this work in order to support the evaluated results.

POTENTIAL MODEL

Thiophene molecules were modeled using a fully flexible atomistic potential. As shown in Fig. 1, thiophene is cyclic with 1-sulfur and 4-carbon atoms in the ring and 4-hydrogens bonded to the carbon atoms. The first 2-carbon atoms bonded to the sulfur atom were labeled as C_1, and the other 2-carbon atoms bonded to C_1 atoms, C_2. Hydrogens were labeled H_1 for those bonded to C_1 atoms and H_2 for those bonded to C_2 atoms.

The geometry, electronic structure, and dipole moment have been reported by Kupka et al. (16) using DFT calculations with the GAUSSIAN 98 software package (22) employing the hybrid potential B3PW91 and the 6-311++G** basis set. Compared to experimental measurements (23), the maximum deviation reported in this work were 0.00087 Angstroms ($S - C_1$) for bond distances, 0.5° ($C_1 - S - C_1$) for valence angles and 0.0408 D for the dipole moment. We used this equilibrium conformation and varied bond distances (±10% from the equilibrium value), valence angles (±10%) and dihedral angles (±90° from the equilibrium value), and performed the same type of calculations but allowing the rest of the atoms

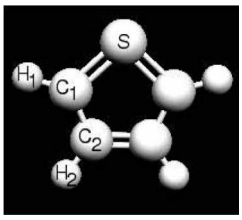

Figure 1. Snapshot of the thiophene molecule.

to relax in order to obtain selected regions of the intramolecular potential energy map of thiophene. The values of the obtained potential energy were fitted to the following expressions of the intramolecular potential:

$$U_{BD}(r_{ij}) = k_{BD}(r_{ij} - r_e)^2 \tag{1}$$

$$U_{VA}(\theta_{ijk}) = k_{VA}(\theta_{ijk} - \theta_e)^2 \tag{2}$$

$$U_{DA}(\phi_{ijkl}) = k_{DA}[\cos(\phi_{ijkl}) - \cos(\phi_e)] \tag{3}$$

where U_{BD}, $U_{VA,}$ and U_{DA} are the potential energy of the bond distance, valence angle and dihedral angle respectively. r_{ij} is the distance between atoms i and j of the same molecule, θ_{ijk} is the valence angle formed by consecutive atoms i, j, and k of the same molecule, ϕ_{ijkl} is the dihedral angle formed by consecutive atoms i, j, k, and l of the same molecule. r_e, θ_e and ϕ_e are the equilibrium values of the bond distance, valence and dihedral angles respectively. k_{BD}, $k_{VA,}$ and k_{DA} are the spring constants of the bond distance, valence, and dihedral angles respectively.

The methodology employed in this work to obtain the parameters of equations (1–3) produced only estimated values of those parameters because, the internal coordinates are correlated and probably such simple expressions will not fit the whole energy map of the molecule. A more appropriated procedure will be first to obtain a grid of the whole potential energy map in terms of combinations of the molecule's internal coordinates, and then use all the obtained points in the grid to fit appropriated expressions of the intramolecular potential. If we propose to study at least 10 points for each bond distance in the molecule, the total number of points to calculate will be 10^9 considering only bond distances, and that is impossible in terms of computational time. The influence of intramolecular forces to the final values of the calculated properties is mixed because even intramolecular forces contribute to the dynamics of the system, they do not contribute to the calculations of properties like pressure or surface tension.

As a graphical example of our results, the calculated potential energies divided by the Boltzmann constant (k_B) as a function of the bond distance $C_1 - C_2$ is shown in Fig. 2 with the best fitted curve of equation (1). Close to the equilibrium separations, the function reproduced well the computed energies, but for a separation of -10% from the equilibrium value, the energy had a difference of $\sim$1000 K. Figures 3 and 4 show the energies and best fitted curves of the valence angle $S - C_1 - C_2$ and the dihedral angle $S - C_1 - C_2 - H_2$, respectively. Valence angles followed similar behavior, close to the equilibrium value the function reproduced well the computed energies, but for a valence angle of -10% from the equilibrium value, a difference of $\sim$1000 K is observed. The fitted curve for the dihedral angle reproduced well the whole range of computed energies, with differences as high as $\sim$100 K at a dihedral angle 90° smaller than the equilibrium value. It is expected that these differences will not affect the simulations due to

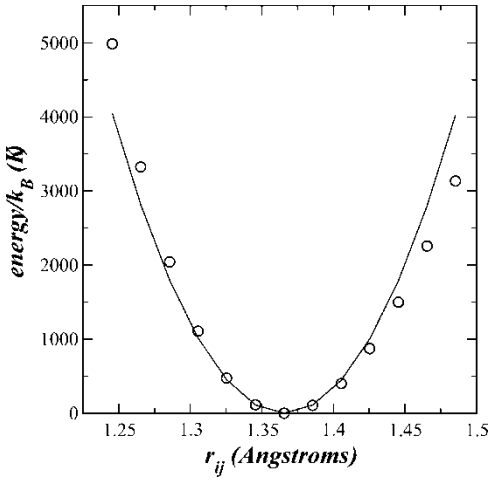

Figure 2. Potential energy curve of thiophene as a function of the bond distance $C_1 - C_2$. Circles represent results of DFT calculations and continuous line represents the best-fitted curve to equation (1).

the fact that the molecules are or tend to return to their equilibrium conformation most of the simulation time. The best fitted parameters for equations (1–3) are reported in Table 1 along with the corresponding equilibrium values.

The intermolecular interactions were modeled as a function of effective pair interactions:

$$U_{Inter}(r_{ij}) = 4\varepsilon_{ij}\left[\left(\frac{\sigma_{ij}}{r_{ij}}\right)^{12} - \left(\frac{\sigma_{ij}}{r_{ij}}\right)^{6}\right] + \frac{q_i q_j}{4\pi\varepsilon_0 r_{ij}} \tag{4}$$

where U_{Inter} is the intermolecular potential energy, r_{ij} is the separation between atoms i and j of different molecules. σ_{ij} and ε_{ij} are the parameters of the Lennard-Jones potential. q_i and q_j are the point charges of the electrostatic potential.

Trokhymchuck and Alejandre (24) had reported that vapor–liquid equilibrium calculations using a spherically truncated Lennard–Jones potential are dependent on the cutoff radius employed in terms of bulk coexistence densities and interfacial properties, and when a cutoff radius of at least $5\sigma_{ij}$ is used, as in this work, the errors in those properties are negligible. The starting Lennard–Jones parameters were taken from the Universal Force Field (UFF) (25) and the Lorentz-Berthelot mixing rules were used for the cross interaction between unlike atoms. The initial plan of this work was to use the information obtained from DFT calculations (geometry, intramolecular parameters, and charges) and optimize the

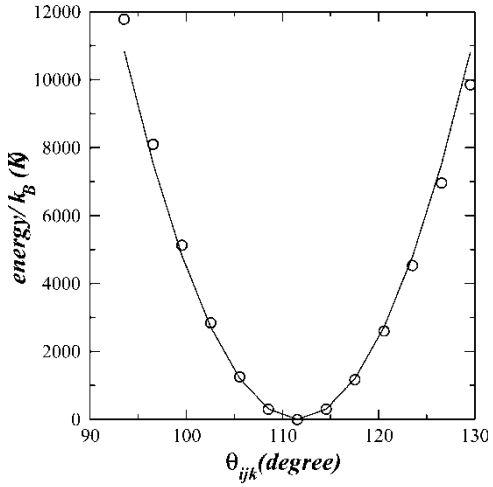

Figure 3. Potential energy curve of thiophene as a function of the valence angle S – C_1 – C_2. Circles represent results of DFT calculations and continuous line represents the best-fitted curve to equation (2).

Lennard-Jones parameters from the UFF and reproduce an experimental result at low temperature, but as shown in the Results Section, the original Lennard-Jones UFF parameters produced a good agreement with the experimental point.

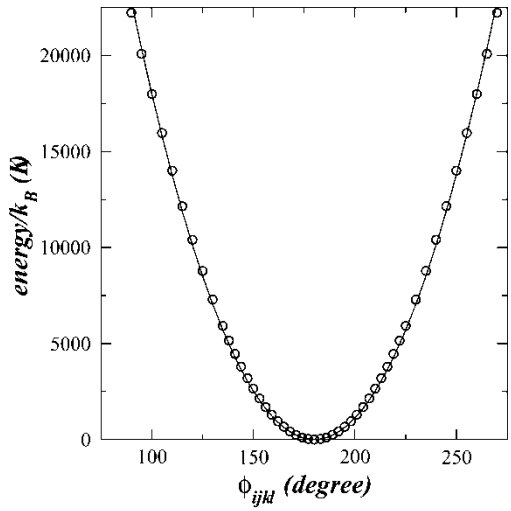

Figure 4. Potential energy curve of thiophene as a function of the dihedral angle S – C_1 – C_2 – H_2. Circles represent results of DFT calculations and continuous line represents the best-fitted curve to equation (3).

Table 1. Computed equilibrium values from DFT calculations and the best fitted values for the parameters k_{BD}, k_{VA} and k_{DA} of equations (1–3). Standard deviations of the residuals between DFT results and fitted functions were computed using the whole set of data (I) and the data corresponding to energies up to 1100 K, (II)

Bond distance	r_{ij} (Angstroms)	k_{BD}/k_B (K)	Standard deviation I	Standard deviation II
$S - C_1$	1.72279	142221	478.143	71.9032
$C_1 - H_1$	1.08019	215237	215.678	32.1133
$C_1 - C_2$	1.36561	280277	448.132	67.1454
$C_2 - H_2$	1.08288	210624	223.457	33.0041
$C_2 - C_2$	1.42411	215264	423.109	60.9344
Valence angle	θ_{ijk} (°)	k_{VA}/k_B (K)		
$S - C_1 - H_1$	120.000	8.90332	281.991	8.71045
$S - C_1 - C_2$	111.551	33.4448	470.444	22.7374
$C_1 - S - C_1$	91.7395	46.5497	468.789	21.2993
$C_1 - C_2 - H_2$	123.323	9.24121	254.098	7.16780
$C_1 - C_2 - C_2$	112.581	31.0999	480.101	23.0108
$H_1 - C_1 - C_2$	128.477	8.60010	268.334	7.25092
$C_2 - C_2 - H_2$	124.102	9.36099	271.786	7.35104
Dihedral angle	ϕ_{ijkl} (°)	k_{DA}/k_B (K)		
$S - C_1 - C_2 - C_2$	0.00000	48795.2	351.393	33.4194
$S - C_1 - C_2 - H_2$	180.000	19365.0	179.062	18.8206
$H_1 - C_1 - S - C_1$	180.000	17698.9	173.674	17.4501
$H_1 - C_1 - C_2 - H_2$	0.00000	10133.5	98.4490	9.45671
$H_1 - C_1 - C_2 - C_2$	180.000	15145.0	123.870	12.4010
$C_1 - C_2 - C_2 - C_1$	0.00000	47912.6	345.069	34.1109
$C_1 - S - C_1 - C_2$	0.00000	69891.0	569.471	68.7041
$C_1 - C_2 - C_2 - H_2$	180.000	18349.4	186.560	17.5601
$H_2 - C_2 - C_2 - H_2$	0.00000	10696.4	99.9811	6.50431

Point charges were computed from the electronic density of the DFT calculations with two common population analysis methodologies, Mulliken (26) and Merz-Singh-Kollman (MSK) (27), and they are reported in Table 2. Point charges were conformation dependent as shown in Fig. 5 for those calculated with the MSK methodology. In Fig. 5a point charges are plotted as a function of the bond distance $C_1 - C_2$, while in Figs 5b and 5c point charges are plotted as a function of valence angle $S - C_1 - C_2$ and dihedral angle $S - C_2 - C_1 - H_2$, respectively. It is interesting that when the bond distance $C_1 - C_2$ is varied, point charges are mostly rearranged between those atoms, while when the valence angle $S - C_1 - C_2$ is perturbed the arrangement of charges is mostly between sulfur and hydrogen atoms, probably because variations in the valence angle produces larger changes in the conformation of the molecule than

Table 2. Computed equilibrium point charges from the DFT calculations and the Mulliken (26) and MSK (27) population analyses

	Point charges (a. u.)	
Atom	Mulliken	MSK
S	−0.2698560	0.0657921
C_1	0.0157355	−0.2476364
C_2	−0.3385865	−0.1479459
H_1	0.2799385	0.2057603
H_2	0.1778405	0.1569252

the variation of one bond distance. The conformation dependency of point charges can be accounted with a weighting factor but due to the fact that our intramolecular potential behavior of Figs. (2)–(4) is almost symmetric with respect to the minima, which correspond to the equilibrium conformation, the new charges were not different from the original. Both set of charges differ in magnitude and in the case of S and C_1 atoms changed sign, such differences had been associated with "buried atoms" in calculations with sulfides and thiols, previously (28).

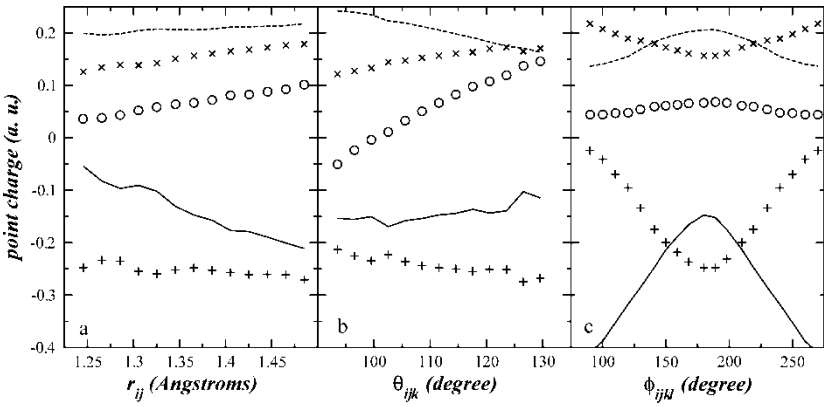

Figure 5. MSK point charges of thiophene as a function of a) the bond distance $C_1 - C_2$, b) the valence angle $S - C_1 - C_2$ and c) the dihedral angle $S - C_1 - C_2 - H_2$. Circles represent sulfur point charge, plus symbols the point charge of the first carbons (C_1) bonded to sulfur atom, continuous line the point charge of carbons (C_2) bonded to C_1 carbons, discontinuous line the point charge of hydrogens (H_1) bonded to C_1 atoms and crosses the point charge of hydrogens (H_2) bonded to C_2 atoms.

SIMULATION DETAILS

Molecular dynamics simulations (NVT-MD) were performed to study the vapor–liquid interface in order to obtain the coexisting densities and interfacial properties (interfacial thickness and surface tension) for pure thiophene using the potential developed in the previous Section with both set of charges. Additional simulations at the corresponding temperature and vapor density were necessary to produce reliable vapor pressure results. This procedure has been successfully employed to simulate pure, binary and ternary non-polar (29, 30), polar (21, 31) polar–non-polar (32) and confined (33) systems. All simulations were carried out using a multiple time step algorithm at constant temperature (34); the fast and slow time steps used were 0.1 and 1 fs respectively. The simulation cells contained 420 molecules of thiophene in the vapor–liquid and 256 in pure vapor. The simulations were performed at temperatures in the range of 300 to 500 K. The dimensions of the simulation cell were $L_x = L_y = 28.82$ Å, and $L_z = 201.77$ Å for liquid–vapor equilibria, and for the pure vapor simulations the dimensions varied with the vapor density. The cutoff radius for Lennard-Jones interactions was 14.38 Å. Electrostatic interactions were handled by the Ewald summation technique with a convergence parameter κ of $5.6/L_x$, and a maximum value for the reciprocal lattice vector h_{max} of 10 (21). After an equilibration period of 150 ps, the averaged properties were then obtained from an additional simulation run of 1 ns.

During simulation, density profiles were calculated in blocks of 10,000 time steps, and at the end the block profiles were averaged. The interfacial thickness and coexistence vapor and liquid densities were obtained through fitting averaged density profiles to a hyperbolic tangent function:

$$\rho(z) = 0.5(\rho_L + \rho_V) - 0.5(\rho_L - \rho_V)\tanh\left[\frac{z - z_0}{d}\right] \tag{5}$$

where ρ_L and ρ_V are the liquid and vapor densities, z_0 is the position of the Gibbs' dividing surface, and d is a parameter related to the thickness of the interface. The actual value of the interfacial thickness t is 2.7192 times the value of the parameter d (32).

The surface tension was calculated using the molecular definition of the pressure tensor (21):

$$\gamma = \frac{L_Z}{2}[\langle P_{ZZ}\rangle - 0.5(\langle P_{XX}\rangle + \langle P_{YY}\rangle)] \tag{6}$$

where $P_{\alpha\alpha}$ is the $\alpha\alpha$ element of the pressure tensor. The factor $1/2$ outside the bracket takes into account the two interfaces in the system. Brackets for each $P_{\alpha\alpha}$ indicate temporal averages. The element $P_{\alpha\alpha}$ of the molecular pressure

tensor for additive pair potentials, as is the case of Lennard-Jones, is given by

$$VP_{\alpha\alpha} = \sum_{i}^{N} m_i (\mathrm{v}_i)_\alpha (\mathrm{v}_i)_\alpha + \sum_{i} \sum_{j>i} \sum_{a} \sum_{b} \left(\mathrm{r}_{iajb}\right)_\alpha \left(\mathrm{f}_{iajb}\right)_\alpha \qquad (7)$$

where N is the number of molecules, V is the volume of the system, m_i is the molecular mass, $(\mathrm{v}_i)_\alpha$ is the velocity of the center of mass in the α-direction, $(\mathrm{r}_{iajb})_\alpha$ and $(\mathrm{f}_{iajb})_\alpha$ are the distance and interaction force between the centers of masses of molecules i and j in the α-direction. For pure component simulations, long-range corrections to the surface tension due to Lennard-Jones interactions beyond the cutoff radius can be estimated (21). For thiophene the expression is given by

$$\gamma_{LRC} = 12\pi\left(\rho_L - \rho_V\right)^2 \sum_{a=1}^{9} \sum_{b=1}^{9} \varepsilon_{ab} \sigma_{ab}^6 \int_0^1 ds \int_{r_C}^{\infty} dr \coth\left(\frac{rs}{d}\right) \frac{\left(3s^3 - s\right)}{r^3} \qquad (8)$$

where ρ_L and ρ_V are the liquid and vapor coexisting densities. ε_{ab} and σ_{ab} are the cross Lennard-Jones parameters. Contributions to the pressure tension due to electrostatic interaction using the Ewald summation technique have been already obtained by Alejandre et al. (21, 35) and were used in this work.

EXPERIMENTAL MEASUREMENTS

Liquid densities of thiophene in the range of 293.31 to 352.44 K were measured experimentally in order to complement and compare them with the simulation results reported. The apparatus used in this work has been previously described by Zúñiga-Moreno et al. (36). The measuring cell is composed of a vibrating tube densitometer (Hastelloy C-276 U-tube) containing 1 cm^3 of sample. The same experimental procedure detailed by Galicia-Luna et al. (38) and by Zúñiga-Moreno and Galicia-Luna (36, 37) is used in this work. The estimated uncertainties are ± 0.03 K for temperatures, ± 0.008 MPa for pressures and $\pm 0.05\%$ for liquid densities. Detailed procedures about calibrations of platinum temperature probes and pressure transducer are given in a previous paper by Zúñiga-Moreno and Galicia-Luna (36). Water and nitrogen were used as reference fluids to calibrate the apparatus. Reference density values of water and nitrogen were obtained with the equations of state (EoS) of Harr et al. (39) and Span et al. (40) respectively. The purity and origin of chemicals used in this work are given in Table 3. They were used without any further purification except for a careful degassing of water and thiophene as in a previous paper (36). New experimental liquid densities of thiophene at atmospheric pressure have been determined at seven temperatures from 293.31 to 352.44 K with an uncertainty lower than $\pm 0.05\%$ and are reported at Table 4. Experimental liquid densities had also

Table 3. Purity and origin of pure compounds

Compound	Reported purity (%)	Supplier
Thiophene	99.0 +	Aldrich
Water	HPLC grade	Aldrich
Nitrogen	99.995	Air products-infra

been reported in the literature at temperatures from 293.15 to 303.15 K by Fawcett and Rasmussen (41) and at 293.15 K by Triday and Rodriguez (42). Our new experimental measurements from 293.31 to 352.44 K reported in this work agreed with interpolated values of those previously reported and also agreed with results using an expression of the DIPPR project (43).

RESULTS

Two different sets of NVT-MD simulations were carried out in the vapor–liquid interface with the corresponding sets of point charges obtained from the population analysis methodologies of Mulliken and MSK. From these simulations, density profiles were obtained at each temperature and as example the profiles at 300 and 500 K are shown in Fig. 6 for both sets of charges. It was not possible to simulate stable vapor–liquid interfaces above 500 K. From the density profiles it is clearly observed that bulk liquid densities obtained with MSK are lower than those obtained with Mulliken charges at the same temperature, while bulk vapor densities obtained with MSK are higher than those obtained with Mulliken charges at the same temperature. In terms of interfacial thickness, it is observed that MSK gives higher values than those obtained with Mulliken charges at the same temperature. At 500 K, all density profiles were almost smooth in the vapor part, while in the

Table 4. Experimental liquid densities for thiophene

Temperature (K)	ρ_L (g/cm^3)
293.31	1.06340
303.05	1.05168
312.84	1.03973
322.74	1.02745
332.65	1.01521
342.53	1.00295
352.44	0.99063

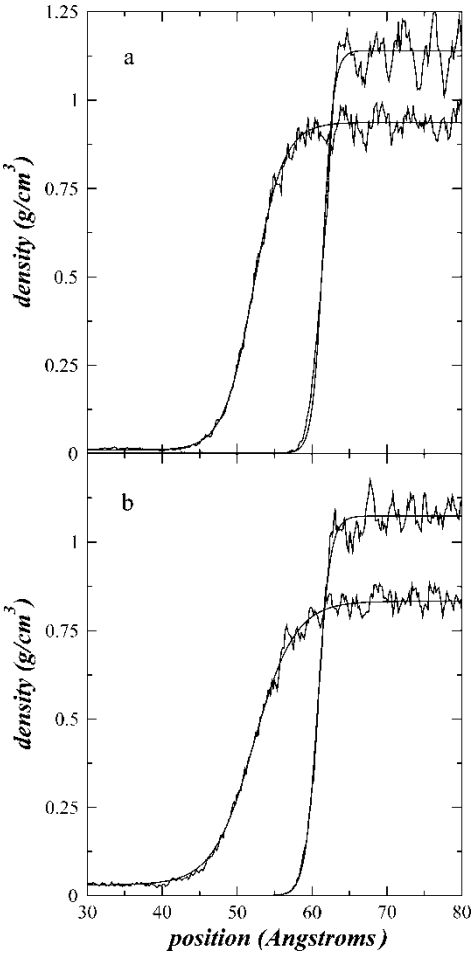

Figure 6. Density profiles of thiophene as a function of the position in the simulation cell using a) Mulliken and b) MSK point charges. Top and bottom curves represent the profiles at 300 and 500 K respectively. Continuous lines represent the best-fitted curves to equation (5).

liquid part variations as big as 0.25 and 0.14 g/cm^3 for the profiles obtained with Mulliken and MSK respectively, were observed. This is probably due to the higher liquid density of Mulliken charges ($\sim$1.14 g/cm^3). At that density, molecules are probably more structured, producing those peaks shown in the bulk liquid phases of Figure 6. In order to show that systems really reached equilibrium configurations, the averages over 100 fs of the potential energy per molecule at 300 K using the MSK charges is shown in Fig. 7. Once the systems reach the equilibration zone, the average potential

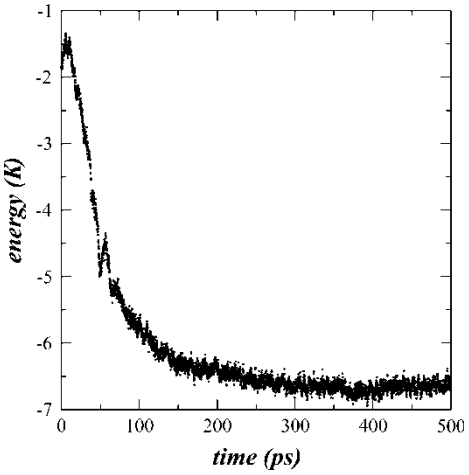

Figure 7. Averaged potential energy per molecule as a function of time for thiophene using MSK charges at 300 K. Each point represents the average potential energy over 100 fs.

energy is -6.6669 K with fluctuations of 0.0791 K calculated as the standard deviation.

Both sets of density profiles were fitted to equation (5) and the vapor and liquid densities are reported in Table 5. The diagram temperature–density is shown in Fig. 8 with both sets of densities. The employed Lennard-Jones parameters with the MSK charges, reproduced the experimental saturated liquid density at 300 K within the simulation error and therefore, there was no need to optimize them. The coexistence points of Mulliken charges will produce a higher critical temperature than those obtained with MSK charges. For comparison, our experimental liquid results along with those of the DIPPR project

Table 5. Simulation results for thiophene. Fitted liquid ρ_L and vapor ρ_V densities, using Mulliken (26) and MSK (27) charges

	Mulliken		MSK	
T (K)	ρ_L (g/cm^3)	ρ_V (g/cm^3)	ρ_L (g/cm^3)	ρ_V (g/cm^3)
300.00	1.141	—	1.074	—
350.00			1.029	—
362.51	1.089	—		
400.00	1.056	0.001	0.968	0.004
450.00	1.008	0.003	0.907	0.009
500.00	0.937	0.010	0.833	0.030

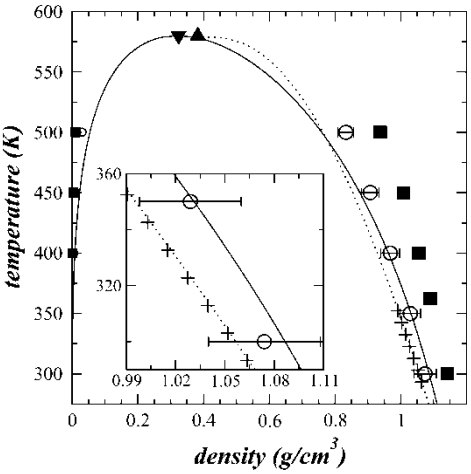

Figure 8. Temperature–density diagram for thiophene. Squares and circles represent the densities calculated in this work using Mulliken and MSK point charges, respectively. Continuous line represents the results using the Peng–Robinson equation of state (44) and the triangle down symbol its predicted critical point. Plus symbols represent our experimental results reported in Table 4 and dotted line represents the results of the DIPPR project (43). Triangle up symbol represents the experimental critical point (45).

are also shown in Fig. 8. Our calculated results for saturated liquid densities using MSK charges at 300 and 350 K are very close to the interpolated values of our experimental liquid densities and agreed with those within the deviation of the simulation results. The coexistence densities were also calculated using the Peng-Robinson equation of state (PR-EOS) (44), a common EOS employed in petroleum engineering. The calculated densities using PR-EOS are also shown in Fig. 8. Our simulation results using the MSK charges agreed well with the PR-EOS results up to 400 K. However, above this temperature the coexistence curve predicted by PR-EOS deviates from the simulation results underestimating liquid densities and overestimating vapor densities at the same temperature. At 300 and 350 K, PR-EOS produced liquid densities with relative errors of $\sim$3% with respect to our experimental interpolated results. The PR-EOS predicted a critical density of $0.324\,\mathrm{g/cm^3}$, whereas Kobe et al. (45) reported an experimental value of $0.382\,\mathrm{g/cm^3}$. It is well known that equations of state predict critical densities or volumes different from the experimental ones (46); to produce reliable liquid density results away from the critical point, EOS have to overpredict the critical density by $\sim$10% (46). In order to determine the real behavior of the coexistence densities in thiophene, experimental measurements, especially between 400 K and the critical temperature are needed.

Table 6. Simulation results for pure thiophene using MSK charges. Average interface thickness t, vapor pressure P_V and surface tension obtained during simulation γ_{SIM}, the long-range correction γ_{LRC} and the total value γ_{TOT}. Numbers between parentheses indicate the precision of the total values

Temperature (K)	t (Å)	P_V (atm)	γ_{SIM} (mN/m)	γ_{LRC} (mN/m)	γ_{TOT} (mN/m)
300	4.526	—	28.74 (3.49)	4.68	33.42 (3.49)
350	6.231	—	24.19 (3.43)	4.11	28.30 (3.43)
400	8.462	3.16 (0.22)	18.74 (3.03)	3.59	22.33 (3.03)
450	11.73	11.03 (0.83)	13.62 (2.98)	3.35	16.97 (2.98)
500	14.86	30.02 (1.04)	10.04 (2.78)	2.51	12.55 (2.78)

The rest of the properties were calculated using only MSK charges because they produced more reliable results for coexisting densities.

Vapor pressures were calculated using equation (7) with the contributions due to electrostatic interactions of the Ewald Summation methodology (21, 35) and are reported in Table 6 for temperatures between 400 and 500 K. At temperatures below 400 K, there are no molecules in the vapor phase even for short periods of time as observed in the density profiles of Fig. 6. The simulation results are shown in Fig. 9 and were compared with those reported in the literature (41, 42, 47). The continuous line represents the best linear regression, fitted using only experimental data. A comparison of the simulation results with an extrapolation of the fitted line showed that

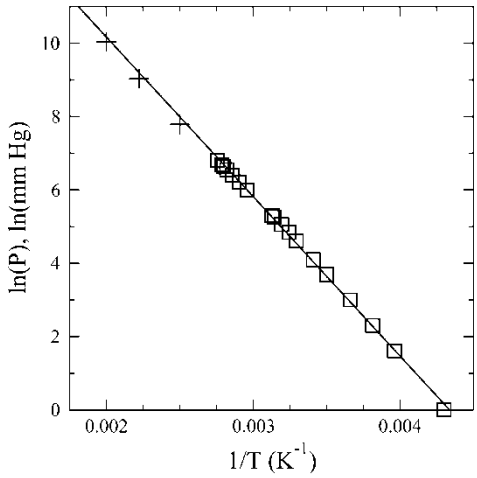

Figure 9. Vapor pressure as a function of temperature for thiophene. Squares represent experimental data (41, 42, 47) and plus symbols represent results of this work. Continuous line represents the linear regression of the experimental values.

the simulation results had the same behavior and agreed well with the extrapolated values. The interfacial thicknesses are also reported in Table 6. They showed similar behavior as other simulation results for polar molecules, where the interfacial thickness increased exponentially with temperature (21, 31); no experimental data has been reported in the literature for this property.

The simulation results for surface tension has two components, the average of surface tension obtained using equation (6) and the contribution due to long-range corrections calculated using equation (8), both contributions are reported in Table 6 along with its total value. The total computed values are shown in Fig. 10 with the experimental results reported by Jasper (48) at 298.15 and 323.15 K. The simulation result at 300 K agreed within the bar error with an interpolated value between the two experimental values. The calculated values showed a regular behavior as other polar molecules (21, 31), the surface tension decreased with the temperature almost linearly. An expression commonly used in engineering to correlate surface tension data is (49):

$$\gamma = A_0\left(1 - \frac{T}{T_C}\right)^{A_1} \tag{9}$$

where the surface tension γ and the parameter A_0 are in mN/m; T and T_C are the temperature and critical temperature respectively in K and A_1 is a dimensionless parameter. Using T_C as another fitting parameter in equation (9), the best set of fitted parameters for the simulation results of the surface tension as

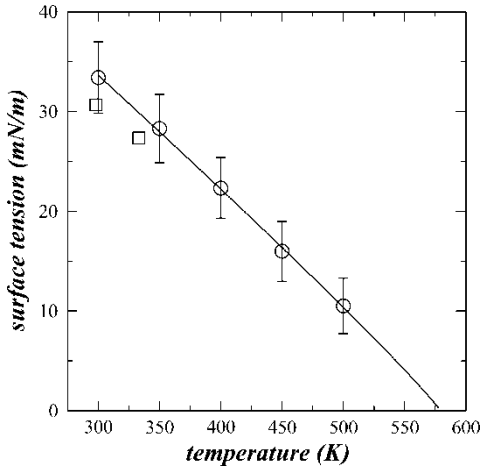

Figure 10. Surface tension as a function of temperature for thiophene. Squares represent experimental data reported by Jasper (48) and circles represent results of this work. Continuous line represents the best fitting curve to equation (9).

a function of temperature, are $A_0 = 66.53\,\mathrm{mN/m}$, $A_1 = 0.9354$ and $T_C = 579.37\,\mathrm{K}$. Compared to the experimental critical temperature reported by Kobe et al. (45), the predicted value has a relative error of 3.46%.

CONCLUSIONS

A new atomistic and fully flexible potential model was developed in this work for the thiophene molecule. The potential model accounted for intra- and intermolecular interactions. The intramolecular part was modeled with three expressions corresponding to the interactions of two, three and four bodies; the parameters of these expressions were obtained trough fitting the intramolecular expressions to the potential energy map, which was generated using DFT calculations. These DFT calculations also produced the most stable geometry and dipole moment of the molecule, which agreed well with experimental results reported in the literature. The intermolecular part was modeled with contributions due to electrostatic interactions and Lennard-Jones interactions. Two sets of parameters for the electrostatic interactions (point charges) were also obtained from the DFT calculations using two different population analysis methodologies of the electronic density, Mulliken, and MSK. These sets of point charges were not weighted with conformations of the molecule because the potential energy map was symmetric with respect to the equilibrium conformations. Lennard-Jones parameters were taken from the Universal Force Field.

The new potential model was tested in the vapor–liquid region using molecular dynamics simulations at the interface. Two different sets of simulations were carried out with the Mulliken and MSK charges respectively. From these simulations, density profiles at the interface at five temperatures were obtained and from those profiles we calculated the coexisting densities for each set of charges and the temperature–density diagram was built. Up to 350 K, no molecules were found in the vapor phase. Simulations with MSK charges produced lower liquid and higher vapor densities than those using Mulliken charges at the same temperature. In order to corroborate our simulation results, new experimental liquid densities were measured from 293.31 to 352.44 K and compared with our simulated results, results using MSK charges are closer than those using Mulliken charges, and the results using MSK charges agreed with our interpolated experimental results within the bar errors. Using an equation of state commonly employed in petroleum engineering, our results agreed up to 400 K, but above this temperature the equation predicted lower liquid and higher vapor densities.

The rest of the properties were calculated using only MSK charges. Interfacial thicknesses were also calculated from the density profiles, following a regular behavior, which is consistent with previous simulations for other polar molecules. Surface tension agreed with the available experimental data at moderate temperatures; a correlation of our results to an expression

commonly used in engineering produced an estimation of the critical temperature 3.46% higher than the experimental point. Independent simulations at the corresponding vapor density and temperature produced reliable vapor pressure data; those results agreed with extrapolated data from experimental values at lower temperatures.

The new potential model developed with MSK charges reproduced well the thermophysical properties studied in this work within the vapor–liquid region. New experimental data is necessary to corroborate the coexisting densities, vapor pressure and surface tension values produced in this work, especially at temperatures from 400 to the critical point.

Future studies will simulate this compound with model oil compounds and supercritical solvent mixtures in order to explore the possibilities of supercritical extraction as a promising method for desulfurization of fuels. We will also perform a systematic study to investigate the orientation and distribution of this molecule close to the interface using a profile of radial distribution functions along the inhomogeneous axis.

ACKNOWLEDGEMENTS

This research was sponsored by PROMEP-SEP (México), the Scientific Research Program (CIC) of the Universidad Michoacana de San Nicolás de Hidalgo, CONACYT and Instituto Politécnico Nacional.

REFERENCES

1. Santamaria-Orozco, D., Horsfield, B., Di Primio, R., and Welte, D.H. (1998) Influence of maturity on distributions of benzo- and dibenzothiophenes in Tithonian source rocks and crude oils, Sonda de Campeche, Mexico. *Org. Geochem.*, 28 (7–8): 423.
2. Colvile, R.N., Hutchinson, E.J., Mindell, J.S., and Warren, R.F. (2001) The transport sector as a source of air pollution. *Atmos. Environ.*, 35 (9): 1537.
3. Cosultchi, A., Garciafigueroa, E., Garcia-Borquez, A., et al. (2001) Petroleum solid adherence on tubing surface. *Fuel*, 80 (13): 1963.
4. Alvarez, L., Espino, J., Ornelas, C., et al. (2004) Comparative study of MoS_2 and Co/MoS_2 catalysts prepared by ex situ in situ activation of ammonium and tetraalkylammonium thiomolybdates. *J. Molec. Catal. A*, 210 (1–2): 105.
5. Espino, J., Alvarez, L., Ornelas, C., et al. (2003) Comparative study of WS_2 and $CodNi/WS_2$ HDS catalysts prepared by ex situ/in situ activation of ammonium thiotungstate. *Catal. Lett.*, 90 (1–2): 71.
6. Song, C. (2003) An overview of new approaches to deep desulfurization for ultraclean gasoline, diesel fuel and jet fuel. *Catal. Today*, 86 (1–4): 211.
7. EPA. (April 13, 2001) Control of air pollution from new motor vehicles amendment for the tier-2/gasoline sulfur regulations, US Environmental Protection Agency. http://www.epa.gov/fedrgstr/EPA-AIR/2001/Apil/Day-13/a8927.htm.

8. EPA. (April, 2003) Reducing air pollution from nonroad engines, US Environmental Protection Agency. http://www.epa.gov/otaq/cleaner-nonroad/f03011.pdf.
9. Castorena, G., Suarez, C., Valdez, I., et al. (2002) Sulfur-selective desulfurization of dibenzothiophene and diesel oil by newly isolated Rhodococcus sp strains. *FEMS Microbiol. Lett.*, 215 (1): 157.
10. Oda, S. and Ohta, H. (2002) Biodesulfurization of dibenzothiophene with Rhodococcus erythropoli ATCC 53968 and its mutant in an interface bioreactor. *J. Biosci. Bioeng.*, 94: 474.
11. Mei, H., Mei, B.W., and Yen, T.F. (2003) A new method for obtaining ultra-low sulfur diesel fuel via ultrasound assisted oxidative desulfurization. *Fuel*, 82 (4): 405.
12. Kim, I.K., Huang, C.P., and Chiu, P.C. (2001) Sonochemical decomposition of dibenzothiophene in aqueous solution. *Wat. Res.*, 35 (18): 4370.
13. Lee, S.H.D., Kumar, R., and Krumpelt, M. (2002) Sulfur removal from diesel fuel-contaminated methanol. *Sep. Purificat. Technol.*, 26 (2–3): 247.
14. Aburto, J. and Le Borgne, S. (2004) Selective adsorption of dibenzothiophene sulfone by an imprinted and stimuli-responsive chitosan hydrogel. *Macromolecules*, 37 (8): 2938.
15. Simandi, B., Sass-Kiss, A., Czukor, B., et al. (2000) Pilot-scale extraction and fractional separation of onion oleoresin using supercritical carbon dioxide. *J. Food Eng.*, 46 (3): 183.
16. Kupka, T., Wrzalik, R., Pasterna, G., and Pasterny, K. (2002) Theoretical DFT and experimental Raman and NMR studies on thiophene, 3-methylthiophene and selenophene. *J. Molec. Struct.*, 616 (1–3): 17.
17. Pasterny, K., Wrzalik, R., Kupka, T., and Pasterna, G. (2002) Theoretical and experimental vibrational studies on liquid thiophene and its acetonitrile solution. *J. Molec. Struct.*, 614 (1–3): 297.
18. Kochikov, I.V., Tarasov, Y.I., Spiridonov, V.P., et al. (2001) The equilibrium structure of thiophene by the combined use of electron diffraction, vibrational spectroscopy and microwave spectroscopy guided by theoretical calculations. *J. Molec. Struct.*, 567 (SI): 29.
19. Soscun, H., Alvarado, Y., Hernandez, J., et al. (2001) Experimental and theoretical determination of the dipole polarizability of dibenzothiophene. *J. Phys. Org. Chem.*, 14 (10): 709.
20. Tsuzuki, S., Honda, K., and Azumi, R. (2002) Model chemistry calculations of thiophene dimer interactions: Origin of pi-stacking. *J. Am. Chem. Soc.*, 124 (41): 12200.
21. Alejandre, J., Rivera, J.L., Mora, M.A., and de la Garza, V. (2000) Force field of monoethanolamine. *J. Phys. Chem. B*, 104 (6): 1332.
22. Frisch, M.J., Trucks, G.W., Schlegel, H.B., et al. (1998) *GAUSSIAN 98, Rev A.6 Program and Manual*; Gaussian, Inc.: Pittsburgh, PA.
23. Kwiatkowski, J.S., Leszczynski, J., and Teca, I. (1997) Molecular structure and infrared spectra of furan, thiophene, selenophene and their 2,5-N and 3,4-N derivatives: density functional theory and conventional post-Hartree-Fock MP2 studies. *J. Molec. Struct.*, 437 (SI): 451.
24. Trokhymchuk, A. and Alejandre, J. (1999) Computer simulations of liquid/vapor interface in Lennard-Jones fluids: Some questions and answers. *J. Chem. Phys.*, 111 (18): 8510.
25. Rappe, A.K., Casewit, C.J., Colwell, K.S., et al. (1992) UFF, a full periodic-table force-field for molecular mechanics and molecular-dynamics simulations. *J. Am. Chem. Soc.*, 114 (25): 10024.

26. Mulliken, R.S. (1955) Electronic population analysis of LCAO-MO molecular wave functions. *J. Chem. Phys.*, 23 (10): 1833.
27. Besler, B.H., Merz, K.M., and Kollman, P.A. (1990) Atomic charges derived from semiempirical methods. *J. Comp. Chem.*, 11 (4): 431.
28. Delhommelle, J., Tschirwitz, C., Ungerer, P., et al. (2000) Derivation of an optimized potential model for phase equilibria (OPPE) for sulfides and thiols. *J. Phys. Chem. B*, 104 (19): 4745.
29. Rivera, J.L. and Alejandre, J. (2002) Vapor–liquid equilibrium simulations of nitrogen and n-alkane binary mixtures. *Coll. Surf A*, 207 (1–3): 223.
30. Rivera, J.L. and Alejandre, J. (2001) Transport properties of nitrogen and n-alkane binary mixtures. *Fluid Phase Equilib.*, 185 (1–2): 389.
31. Rivera, J.L., Predota, M., Chialvo, A.A., and Cummings, P.T. (2002) Vapor–liquid equilibrium simulations of the SCPDP model of water. *Chem. Phys. Lett.*, 357 (3–4): 189.
32. Rivera, J.L., McCabe, M., and Cummings, P.T. (2003) Molecular simulations of liquid–liquid interfacial properties: Water-n-alkane and water-methanol-n-alkane systems. *Phys. Rev. E*, 67 (1): 011603.
33. Rivera, J.L., McCabe, M., and Cummings, P.T. (2002) Layering behavior and axial phase equilibria of pure water and water plus carbon dioxide inside single wall carbon nanotubes. *Nano Lett.*, 2 (12): 1427.
34. Tuckerman, M., Berne, B.J., and Martyna, G.J. (1992) Reversible multimple time scale molecular-dynamics. *J. Chem. Phys.*, 97 (3): 1990.
35. Alejandre, J., Tildesley, D.J., and Chapela, G.A. (1995) Molecular-dynamics simulation of the orthobaric densities and surface tension of water. *J. Chem. Phys.*, 102 (11): 4574.
36. Zúñiga-Moreno, A. and Galicia-Luna, L.A. (2002) Densities of 1-propanol and 2-propanol via a vibrating tube densimeter from 313 to 363 K and up to 25 MPa. *J. Chem. Eng. Data*, 47 (2): 155.
37. Zúñiga-Moreno, A. and Galicia-Luna, L.A. (2002) Compressed liquid densities of carbon dioxide plus ethanol mixtures at four compositions via a vibrating tube densimeter up to 363 K and 25 MPa. *J. Chem. Eng. Data*, 47 (2): 149.
38. GaliciaLuna, L.A., Richon, D., and Renon, H. (1994) New loading technique for a vibrating tube densimeter and measurements of liquid densities up to 39.5 MPa for binary and ternary mixtures of the carbon-dioxide methanol propane system. *J. Chem. Eng. Data*, 39 (3): 424.
39. Haar, L., Gallager, J.S., and Kell, G.S.A. (1984) *NBS/NRC Steam Tables*; McGraw Hill: New York.
40. Span, R., Lemmon, E.W., Jacobsen, R.T., and Wagner, W. (1998) A reference quality equation of state for nitrogen. *Int. J. Thermophys.*, 19 (4): 1121.
41. Fawcett, F.S. and Rasmussen, H.E. (1945) Physical properties of thiophene. *J. Am. Chem. Soc.*, 67 (10): 1705.
42. Triday, J.O. and Rodriguez, P. (1985) Vapor–liquid equlibria for the system benzene thiophene methanol. *J. Chem. Eng. Data.*, 30 (1): 112.
43. Wilding, W.V., Rowley, R.L., and Oscarson, J.L. (1998) DIPPR (R) Project 801 evaluated process design data. *Fluid Phase Equilib.*, 150–151: 413.
44. Peng, D. and Robinson, D.B. (1976) New 2-constant equation of state. *Ind. Eng. Chem. Fundam.*, 15 (1): 59.
45. Kobe, K.A., Ravicz, A.E., and Vohra, S.P. (1956) Critical properties and vapor pressures of some ethers and heterocyclic compounds. *Ind. Eng. Chem., Chem. Eng. Data Series*, 1 (1): 50.

46. Teja, A.S., Smith, R.L., and Sandler, S.I. (1983) The calculation of critical-points of fluid mixtures–effect of improved pure component critical-point representation. *Fluid Phase Equilib.*, 14: 265.
47. Liley, P.E., Thomson, G.H., Friend, D.G., et al. (1997) *Perry's Chemical Engineers' Handbook*; McGraw Hill: Int. Ed.
48. Jasper, J.J. (1972) The surface tension of pure liquid compounds. *J. Phys. Chem. Ref. Data*, 1 (4): 841.
49. Yaws, C.L., Lin, X., Bu, L., and Nijhawan, S. (1999) *Chemical Properties Handbook*; McGraw-Hill: Int. Ed.